

Detecting Effects of Filaments on Galaxy Properties in the Sloan Digital Sky Survey III

Yen-Chi Chen,^{1,3*} Shirley Ho,^{2,3} Rachel Mandelbaum,^{2,3} Neta A. Bahcall,⁴
Joel R. Brownstein,⁵ Peter E. Freeman,^{1,3} Christopher R. Genovese,^{1,3}
Donald P. Schneider,^{6,7} Larry Wasserman^{1,3}

¹*Department of Statistics, Carnegie Mellon University, Pittsburgh, PA 15213, USA*

²*Department of Physics, Carnegie Mellon University, Pittsburgh, PA 15213, USA*

³*McWilliams Center for Cosmology, Carnegie Mellon University, Pittsburgh, PA 15213, USA*

⁴*Department of Astrophysical Sciences, Princeton University, Princeton, NJ, 08544, USA*

⁵*Department of Physics and Astronomy, University of Utah, 115 S 1400 E, Salt Lake City, UT 84112, USA*

⁶*Department of Astronomy and Astrophysics, The Pennsylvania State University, University Park, PA 16802, USA*

⁷*Institute for Gravitation and the Cosmos, The Pennsylvania State University, University Park, PA 16802, USA*

28 June 2022

ABSTRACT

We study the effects of filaments on galaxy properties in the Sloan Digital Sky Survey (SDSS) Data Release 12 using filaments from the ‘Cosmic Web Reconstruction’ catalogue (Chen et al. 2015a), a publicly available filament catalogue for SDSS. Since filaments are tracers of medium-to-high density regions, we expect that galaxy properties associated with the environment are dependent on the distance to the nearest filament. Our analysis demonstrates that a red galaxy or a high-mass galaxy tend to reside closer to filaments than a blue or low-mass galaxy. After adjusting the effect from stellar mass, on average, late-forming galaxies or large galaxies have a shorter distance to filaments than early-forming galaxies or small galaxies. For the Main galaxy sample, all signals are very significant ($> 5\sigma$). For the LOWZ and CMASS samples, most of the signals are significant (with $> 3\sigma$). The filament effects we observe persist until $z = 0.7$ (the edge of the CMASS sample). Comparing our results to those using the galaxy distances from redMaPPer galaxy clusters as a reference, we find a similar result between filaments and clusters. Our findings illustrate the strong correlation of galaxy properties with proximity to density ridges, strongly supporting the claim that density ridges are good tracers of filaments.

Key words: (cosmology:) large-scale structure of Universe – galaxies: general

1 INTRODUCTION

Matter in our Universe tends to aggregate around certain low-dimensional structures that form the Universe into a network called the cosmic web (Bond et al. 1996). The cosmic web consists of four distinct types of sub-structures: highly concentrated clusters, elongated filaments, widely spread sheets, and voids. In this study, we focus on filaments for three reasons. First, a large fraction of the matter in the Universe is contained in and around filaments (Aragón-Calvo et al. 2010; Eardley et al. 2015), allowing detection of the correlation between filaments and properties of nearby galaxies even when the correlation is weak. Second, filaments are similar to clusters in the sense that they both occupy

higher density regions (in comparison to walls and voids). We therefore expect galaxies close to filaments to share some characteristics of galaxies around clusters. Lastly, relatively few studies have been performed for filaments compared to clusters (some recent work can be found in Tempel et al. 2014b; Guo et al. 2015; Tempel et al. 2015; Zhang et al. 2015).

Despite the vagueness of the formal definition of filaments, they are typically described as curve-like tracers of high-density regions of the Universe (Bond et al. 1996). As studies of galaxy clusters have shown, galaxy properties are dependent on the density of the environment (Butcher & Oemler 1978; Bower et al. 1992). We are therefore interested whether similar trends exist for galaxies in or around filaments.

Vast amounts of evidence demonstrate that the environ-

* E-mail: yenchic@andrew.cmu.edu

ment around a galaxy affects that galaxy's star formation; see, e.g., Kauffmann et al. (2004); Blanton et al. (2005b); Christlein & Zabludoff (2005); González & Padilla (2009). Moreover, direct evidence also suggests that star formation is related to the nearby filaments (Darvish et al. 2014). Hence, galaxy properties related to star formation, such as the color, number of satellites, stellar mass and disk galaxy spin alignment (Robertson et al. 2005; Lagos et al. 2009; González & Padilla 2009; Guo et al. 2015; Codis et al. 2015), are expected to be influenced by the environment. In particular, direct evidence has indicated that a galaxy's color is generally correlated with the environment; see, e.g., Hogg et al. (2003); Balogh et al. (2004); Springel et al. (2005); Park et al. (2007); Coil et al. (2008); Font et al. (2008); Guo et al. (2011). These findings suggest that red galaxies tend to reside in high-density regions while blue galaxies tend to live in low-density regions (Cowan & Ivezić 2008; Grützbauch et al. 2011).

In addition to the color, other quantities such as stellar mass, size and age of a galaxy are related to the environment. Grützbauch et al. (2011) found that stellar mass is correlated with the local density, i.e., galaxies located in high-density regions tend to be more massive. Moreover, direct evidence reported by the GAMA (Galaxy And Mass Assembly) survey has shown that galaxies within different environments have different stellar mass distributions (Alpaslan et al. 2015). Indirect evidence also links the stellar mass to the environment by the stellar mass-halo mass ratio (Moster et al. 2010) and the fact that environment impacts halo formation (Desjacques 2008). The size-environment relation has been observed in Cooper et al. (2012) and Lani et al. (2013), and the environment is also correlated with the Fundamental Plane relating velocity dispersion, surface brightness, and size of elliptical galaxies (Joachimi et al. 2015). Moreover, the size-stellar mass relation is dependent on the environment (Cappellari 2013; Kelkar et al. 2015). In addition to stellar mass and size, many studies have shown that the age of a galaxy is environment-dependent; see e.g. (Bernardi et al. 1998; Trager et al. 2000; Sil'chenko 2006; Bernardi et al. 2006; Wegner & Grogin 2008; Smith et al. 2012a; Deng 2014). Since filaments are tracers of medium-to-high density regions, we expect that all these galaxy properties are correlated with proximity to filaments as well.

Besides the above galaxy properties, due to the tidal and velocity field around filaments (Hahn et al. 2007a,b; Tempel et al. 2014a), spin and principal axes of a galaxy are known to be correlated with orientation of nearby filaments, see, e.g., Altay et al. (2006); Tempel et al. (2013); Tempel & Libeskind (2013); Aragón-Calvo & Yang (2014); Dubois et al. (2014); Chen et al. (2015b). However, in the current paper, we focus only on the the color, stellar mass, age, and size of a galaxy and study how these properties may be related to the distance to filaments.

The fact that galaxies around filaments and clusters share some characteristics can be used to test the consistency of a filament finding technique. An issue for filament detection is that there is no consensus on the precise definition of filaments. There is only a general, qualitative agreement that they are curve-like structures that trace high-density regions (Bond et al. 1996). The term high-density is used here is to compare with cosmic sheets or voids. Most of the current state-of-the-art filament finders, such as the

Multiscale Morphology Filter (MMF; Aragón-Calvo et al. 2007, 2010), the NEXUS and NEXUS+ (Cautun et al. 2013), the Candy model (Stoica et al. 2007; Stoica et al. 2005), the skeleton (Novikov et al. 2006; Sousbie et al. 2008a,b), and the DisPerSE models (Sousbie 2011), all output filaments consistent with this high-density property. Comparing a new filament finder to the existing ones may not be an optimal way to check the consistency of detecting real filaments; a better approach is to compare the properties of those galaxies that are around the filaments since, in theory, these galaxies should be similar to those close to clusters.

In this paper, we study properties of Sloan Digital Sky Survey (SDSS York et al. 2000; Eisenstein et al. 2011) galaxies around filaments up to $z = 0.7$ using the 'Cosmic Web Reconstruction' filament catalogue (Chen et al. 2015a). Previous studies for filaments in SDSS mostly used the Main galaxy sample (Strauss et al. 2002) with $z \leq 0.25$ (Bond et al. 2010; Jasche et al. 2010; Smith et al. 2012b; Zhang et al. 2015; Leclercq et al. 2015). Generally, finding filaments beyond the Main galaxy sample catalogue is challenging due to the low observational number density, which decreases the detection accuracy drastically. By using density ridges as filaments (Chen et al. 2015c; Chen et al. 2015a) and a process of redshift-slicing the Universe, the power of detecting filaments increases, which allows us to study the correlation between filaments and their nearby galaxies.

This paper is organized as follows. We begin with an introduction to the SDSS dataset in §2 and the filament catalogue in §3. We present our results for separating galaxies by the color (§4), stellar mass (§5), age (§6), and size (§7). Finally, we conclude this paper in §8.

We assume a WMAP7 Λ CDM cosmology with $H_0 = 70$, $\Omega_m = 0.274$, and $\Omega_\Lambda = 0.726$ (Anderson et al. 2012, 2014a).

2 THE SDSS DATA

We use three catalogs from SDSS data that contain the Main galaxy sample (MGS) from DR7 (Abazajian et al. 2009), and LOWZ and CMASS samples from DR12 (Alam et al. 2015).

SDSS I, II, and III together scanned $14,555 \text{ deg}^2$ of the sky using a five-band (u, g, r, i, z) photometric bandpasses (Fukugita et al. 1996; Doi et al. 2010) to a limiting magnitude of $r \simeq 22.5$. The resulting image data were then processed through a sequence of pipelines including astrometric calibration (Pier et al. 2003), photometric reduction (Lupton et al. 2001), and photometric calibration (Padmanabhan et al. 2008).

The SDSS DR7 (Abazajian et al. 2009) consists of the completed data set of SDSS-I and SDSS-II. These two surveys obtained wide-field CCD photometry (Gunn et al. 1998, 2006) in u, g, r, i, z photometric bandpasses (Fukugita et al. 1996; Doi et al. 2010), internally calibrated using the 'uber-calibration' process as described in Padmanabhan et al. (2008), forming a total footprint of $11,663 \text{ deg}^2$ of the sky. Based on the imaging data, galaxies within a region of 9380 deg^2 (Abazajian et al. 2009) were further selected for spectroscopic observation as part of the main galaxy sample (MGS; Strauss et al. 2002), which contains all galaxies with $r_{\text{pet}} < 17.77$, where r_{pet} is the extinction-corrected r -band Petrosian magnitude.

We obtain the SDSS DR7 MGS from the NYU value-

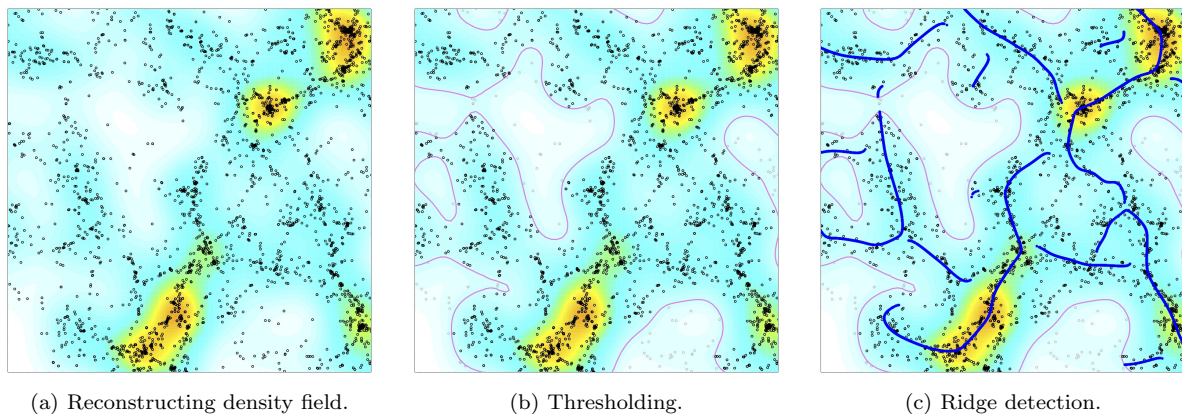


Figure 1. An example of identifying filaments using the density ridge model. Our filament catalogue uses the density ridge model to trace filaments. The catalogue is obtained by applying SCMS algorithm, which consists of three steps: reconstructing density (panel (a)), thresholding low-density regions (panel (b)), and detecting density ridges (blue curves in panel (c)).

added catalogue (NYU VAGC, Blanton et al. 2005a; Padmanabhan et al. 2008; Adelman-McCarthy et al. 2008). The NYU VAGC includes K-corrected absolute magnitudes, and detailed information on the mask. This dataset uses galaxies with $14.5 < r_{\text{pet}} < 17.6$. The lower limit ($r_{\text{pet}} > 14.5$) guarantees that only galaxies with reliable SDSS photometry are included and the upper limit ($r_{\text{pet}} < 17.6$) gives a homogeneous selection over the full footprint of 6141 deg^2 (Blanton et al. 2005a). For galaxies that did not obtain a redshift due to fibre collisions, we assign their redshift according to the nearest neighbor.

The LOWZ and CMASS samples are from Data Release 12 (Alam et al. 2015), the final data of SDSS-III. The Baryon Oscillation Spectroscopic Survey (BOSS) of SDSS-III has obtained spectra and redshifts for around 1.35 million galaxies over a region covering 10,000 square degrees of the sky. These galaxies were selected based on the SDSS imaging (Aihara et al. 2011) and observed along with 160,000 quasars and approximately 100,000 ancillary targets. The targets are assigned to tiles of diameter 3 degrees using the algorithm in Blanton et al. (2003) that adopts to the target density on the sky (Blanton et al. 2003). Spectra are obtained from the BOSS spectrographs (Smei et al. 2013). Each observation is then applied a series of 15-minute exposures, integrating signals until a signal-to-noise ratio threshold is passed for the faint galaxies. This approach yields a homogeneous data set with a high redshift completeness (more than 97%) over the full survey footprint. Finally, redshifts are extracted from the spectra using the approach described in Bolton et al. (2012). A summary of the survey design can be found in Eisenstein et al. (2011); a full description of BOSS is in Dawson et al. (2013).

BOSS selects two different classes of galaxies for spectroscopy : ‘LOWZ’ and ‘CMASS’; detailed description for these two classes can be found in Anderson et al. 2014a. For the LOWZ sample, the effective redshift is $z_{\text{eff}} = 0.32$, as we apply a redshift cut $z < 0.43$. The CMASS sample has a median redshift $z = 0.57$ and a stellar mass distribution with maximum at $\log_{10}(M/M_{\odot}) = 11.3$ (Maraston et al. 2013). The majority of CMASS sample are central galaxies located in dark matter haloes of mass $\sim 10^{13} h^{-1} M_{\odot}$.

3 THE FILAMENT CATALOGUE

In this paper, we apply the ‘Cosmic Web Reconstruction’ catalogue (Chen et al. 2015a), a publicly available filament catalogue, to study properties of galaxies around filaments¹. Below we briefly summarize its construction.

The filament catalogue consists of filaments within 130 slices of the Universe from redshift $z = 0.050$ to $z = 0.700$, with slice width $\Delta z = 0.005$ (Chen et al. 2015a). Filaments in each slice are obtained by applying a three-stage procedure (Chen et al. 2015c; Chen et al. 2015a), as explained in the follows.

For each slice, we first smooth galaxies within this slice into a density field. This procedure is done by the kernel density estimator (KDE); namely, the density is given by

$$p(x) = \frac{1}{nb^2} \sum_{i=1}^N K\left(\frac{\|x - X_i\|}{b}\right), \quad (1)$$

where X_i is the $(\alpha_{2000}, \delta_{2000})$ coordinate for i -th galaxy within this slice, and N is the total number of galaxies in this slice, and b is the smoothing parameter selected using the rule described in Chen et al. (2015a). After reconstructing the density field, we remove galaxies whose density value is below $\lambda = p_{\text{rms}}$. Lastly, we apply the subspace constrained mean shift algorithm (SCMS Ozertem & Erdogmus 2011) based on galaxies pass the density threshold λ to obtain filaments. The SCMS detects filaments as ridges (Eberly 1996; Genovese et al. 2014; Chen et al. 2014, 2015c) of the density function in equation (1). Figure 1 provides an illustration of the above process used to construct filaments from given galaxies’ positions. More detailed implementation for the filament detection algorithm can be found in Chen et al. (2015a).

By applying the above procedure to each of the 130 slices, we construct a filament catalogue ranging from $z = 0.050$ to $z = 0.700$. We provide examples for detected filaments in the range of Main galaxy sample (MGS), LOWZ and CMASS in Figure 2.

¹ The catalogue can be downloaded from <https://sites.google.com/site/yenchicr/catalogue>.

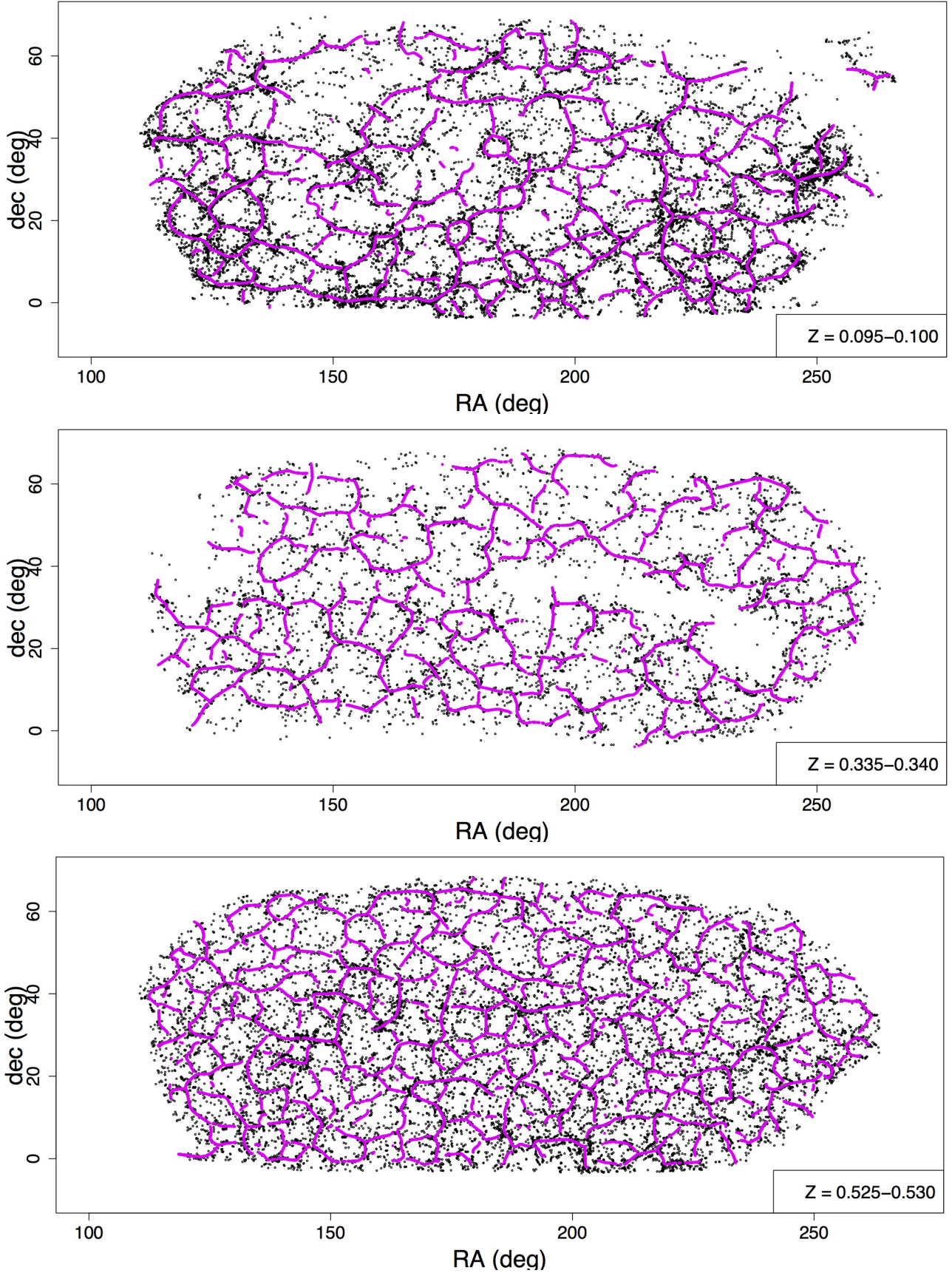


Figure 2. Examples of the filament catalogue in narrow redshift slices within the MGS, LOWZ, and CMASS samples, respectively. In all panels, we observe that galaxies are indeed concentrate around filaments.

Table 1. Definition of Parameters.

Parameters	Definition	Comment
d_F	Distance to the nearest filament.	
d_C	Distance to the nearest cluster.	
$\langle d_F \rangle_{\text{total}}$	Average d_F within each redshift slice.	Figure 3 and 4.
$\langle d_C \rangle_{\text{total}}$	Average d_C within each redshift slice.	Figure 3 and 4.
$\langle d_F \rangle_{\text{mass,total}}$	Average d_F within each redshift slice and each fine mass bin.	Figure 5 and 6.
$\langle d_C \rangle_{\text{mass,total}}$	Average d_C within each redshift slice and each fine mass bin.	Figure 5 and 6.

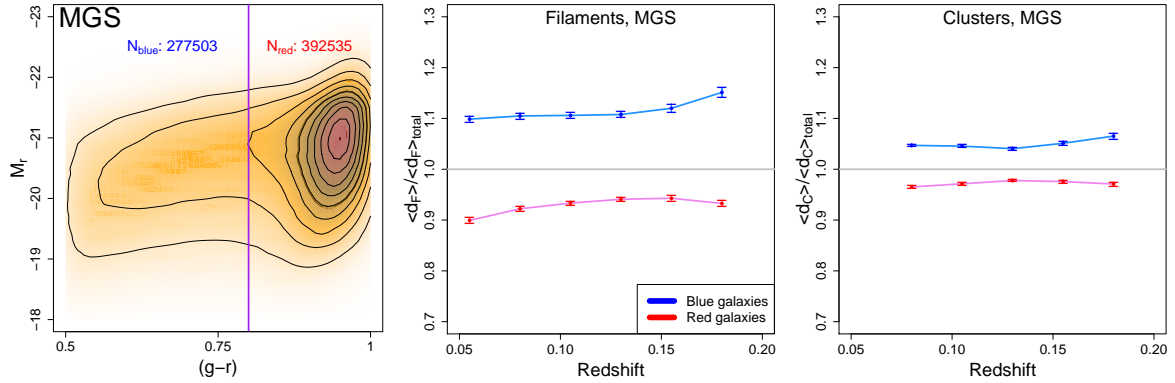


Figure 3. The difference between the proximity to filaments (and clusters) from red and blue galaxies in the Main galaxy sample (MGS) with $z \leq 0.2$. **Left panel:** the color-magnitude diagram. The purple line indicates the color cut we use for separating blue (total number $N_{\text{blue}} = 277,503$) and red galaxies (total number $N_{\text{red}} = 392,536$). **Center panel:** Scaled distance from red and blue galaxies to filaments. **Right panel:** Scaled distance from red and blue galaxies to clusters. In both center and right panels, blue curves are significantly above red curves, indicating that blue galaxies, on average, have a larger distance to both filaments and clusters than red galaxies.

4 RESULTS: COLOR

Observational evidence suggests that the color of a galaxy is generally dependent on the environment in which this galaxy resides (Springel et al. 2005; Coil et al. 2008; Cowan & Ivezić 2008; Font et al. 2008; Guo et al. 2011; Grützbauch et al. 2011). If filaments from density ridges trace the high-density environments well, there should be more red galaxies around or in filaments than blue galaxies.

To define red and blue galaxies, we use a simple cut such that a galaxy is classified as a red galaxy if $(g-r) > 0.8$ and is a blue galaxy otherwise. The k-correction is used to correct to a standard redshift of $z = 0.1$. The first panel in Figure 3 shows the color cut in the color-magnitude diagram. In this comparison, we only use the MGS sample since most galaxies in the LOWZ and CMASS sample are red galaxies (blue galaxies were not selected for spectroscopy for the LOWZ and CMASS sample).

We then compare the average distance to filaments (and clusters) from blue and red galaxies at different redshift regions, denoting d_F and d_C as the distances from a galaxy to its nearest filament and cluster, respectively. This distance is based on 2D projection within each redshift slice. The galaxy clusters are taken from redMaPPer cluster catalogue version 5.10 (Rykoff et al. 2014; Rozo & Rykoff 2014; Rozo et al. 2015).

In particular, we compare the scaled distance to fila-

ments (and clusters). The scaled distance is obtained by dividing the distance to filaments (and clusters) by the average distance from all galaxies, i.e., we compare

$$d_F / \langle d_F \rangle_{\text{total}}, \quad d_C / \langle d_C \rangle_{\text{total}} \quad (2)$$

from both blue and red populations. The two quantities

$$\langle d_F \rangle_{\text{total}}, \quad \langle d_C \rangle_{\text{total}} \quad (3)$$

are the average distance to filaments and clusters for a given subsample by the average distance from all galaxies within the same redshift slice. We include the definitions for the above quantities in Table 1 for reference. We normalize the distance for two reasons. We are only interested in detecting if two populations have different average distances. Scaling the distance by the average over all galaxies does not change the significance of differences between the populations. Due to the change in the number density with redshift in the SDSS, the average distance between a pair of galaxies and the distance to filaments or clusters from a galaxy are changing (the average distance to filaments at different redshifts can be found in Chen et al. 2015a). Without correcting for this effect, the average distance as a function of redshift is difficult to interpret. Scaling the distance by the average over all galaxies eliminates this problem.

The center and right panels of Figure 3 display the results for comparing red and blue galaxies. When we compute the average distance, we only consider the average distance

for galaxies whose distance is less than 100 Mpc, i.e., for averaging distance to filaments, we are actually taking the average over galaxies whose distance to filaments is less than 100 Mpc; a similar computation works for clusters. We apply this distance cut to avoid galaxies that are located at too great a distance.

The center and right panels of Figure 3 reveal a clear pattern that the red and blue galaxies have significantly different average distances to both filaments and clusters (this separation has a 57σ significance; see Table 2); the red galaxies are closer to filaments and clusters compared to blue galaxies. Our result is qualitatively consistent with the existing literature; see, e.g., Hogg et al. (2003); Cowan & Ivezić (2008); Grützbauch et al. (2011). Figure 3 only displays the contrast between red and blue galaxies. We do not calibrate the effect of number density, so that one cannot interpret the result in Figure 3 as an evidence for the evolution of the correlation between filaments and galaxy color across different redshifts.

The significance for comparing average distance to filaments from red and blue galaxies is computed as follows. For each slice in MGS, say slice ℓ , let $\langle d_F \rangle_{\text{red},\ell}$ and $\langle d_F \rangle_{\text{blue},\ell}$ denote the average distance (without scaling) to filaments from red and blue populations. The quantities $\sigma_{\text{red},\ell}$ and $\sigma_{\text{blue},\ell}$ are the standard errors for $\langle d_F \rangle_{\text{red},\ell}$ and $\langle d_F \rangle_{\text{blue},\ell}$ respectively (standard errors are computed using variance of sample average). Let S_{MGS} represent the number of slices in MGS (in our case, $S_{\text{MGS}} = 30$). We use the statistic

$$T_{\text{color,MGS}} = \frac{1}{\sqrt{S_{\text{MGS}}}} \sum_{\ell=1}^{S_{\text{MGS}}} \frac{\langle d_F \rangle_{\text{blue},\ell} - \langle d_F \rangle_{\text{red},\ell}}{\sqrt{\sigma_{\text{red},\ell}^2 + \sigma_{\text{blue},\ell}^2}} \quad (4)$$

to measure the significance for the difference in red and blue populations. If the color is not correlated with distance to filaments, the distribution for the distance from both red and blue populations will be the same, so that $T_{\text{color,MGS}}$ follows a standard normal distribution (mean 0, variance 1) asymptotically. Our computation shows a 58σ significance for comparing red and blue galaxies. The statistic in equation 4 stacks signals from each slice to enhance the overall signal so that the significance is strong. We also run a KS test and the resulting p-value is similar to the above method.

An interesting pattern is that the difference between blue and red galaxies is larger for filaments than clusters. There are two possible reasons for this. First, the total number of reMaPPer clusters in the MGS region is relatively small compared to the number of filaments. Therefore, the effective number of galaxies that are influenced by clusters is small. Those galaxies that are located at great distances from clusters contribute only to $\langle d_C \rangle_{\text{total}}$, not the separation between red and blue galaxies. Thus, when we divide d_C by $\langle d_C \rangle_{\text{total}}$, the denominator increases, which flattens the separation. Second, filaments are curves that have dimension 1 while clusters are points. There will be more galaxies around filaments compared to the number of galaxies around clusters. Those galaxies close to filaments (or clusters) contribute to the separation between red and blue galaxies, while galaxies at large distance from filaments (or clusters) only contribute to the total average $\langle d_F \rangle_{\text{total}}$ (or $\langle d_C \rangle_{\text{total}}$). As a result, the separation between red and blue galaxies will appear to be stronger for filaments.

5 RESULTS: STELLAR MASS

In galaxy evolution, one of the most important properties is the stellar mass of a galaxy. Grützbauch et al. (2011) and Alpaslan et al. (2015) found that the stellar mass of a galaxy depends on the environment. Since filaments are tracers of the overdense regions, we expect to see the average distance to filaments from galaxies to be different when galaxies are partitioned according to their stellar mass.

To obtain the stellar mass for each SDSS galaxy, we use the result from the Granada Group. The Granada Group applies the Flexible Stellar Population Synthesis (FSPS) code (Conroy et al. 2009) to SDSS DR12, computing the stellar mass and age for each galaxy².

The panels in the first column of Figure 4 display the distribution of stellar mass at different redshifts for each catalogue. We divide galaxies into three mass bins: low-mass, moderate-mass, and high-mass galaxies. Since the mass distribution is different from each catalogue, we use different mass cuts for different catalogues. The mass cuts are chosen to balance the number of galaxies within each bin. The two horizontal black lines in each panel of the first column panels of Figure 4 are the mass cuts.

For each mass bin and each catalogue, we perform the same analysis as in analyzing the color: we first scale the distance within each slice by the average distance from all galaxies and then compute the distance from different galaxies in different mass bin. For the Main galaxy sample (MGS), we only consider $z \leq 0.20$; for the LOWZ sample, we focus on $0.20 \leq z \leq 0.43$; for the CMASS sample, we include $0.43 \leq z$. The two vertical dashed lines in each panel indicate the boundaries of MGS, LOWZ and CMASS. The two redshift cuts ($z = 0.20, 0.43$) are based on the number density for each catalogue; see Anderson et al. (2014b).

The center and middle columns of Figure 4 display the results. For the proximity to filaments (center column), the average scaled distances in the three mass bins significantly differ from one another. We observe significances $> 3\sigma$ using the same formula as in equation (4), indicating that high-mass galaxies tend to appear around filaments than the low-mass galaxies, i.e., a galaxy's stellar mass is correlated with its proximity to filaments.

The right column of Figure 4 presents the same analysis for clusters. We find a clear pattern: the three mass bins have different distances to clusters on average, indicating that stellar mass is correlated with the proximity to clusters. Comparing the result for clusters to filaments indirectly demonstrates that in all three samples, the difference between high-mass galaxies and low-mass galaxies is larger in the cluster case than in the filament case at the LOWZ and CMASS sample. This result is reasonable since clusters are tracers of the extremely dense regions, while filaments are tracers of regions with a mild overdensity compared to clusters. Since galaxies that reside in high-density regions tend to have more stellar mass (Grützbauch et al. 2011), we expect the high-mass galaxies have a higher change to appear around clusters than low-mass galaxies.

² More details can be found in http://www.sdss.org/dr12/spectro/galaxy_granada/

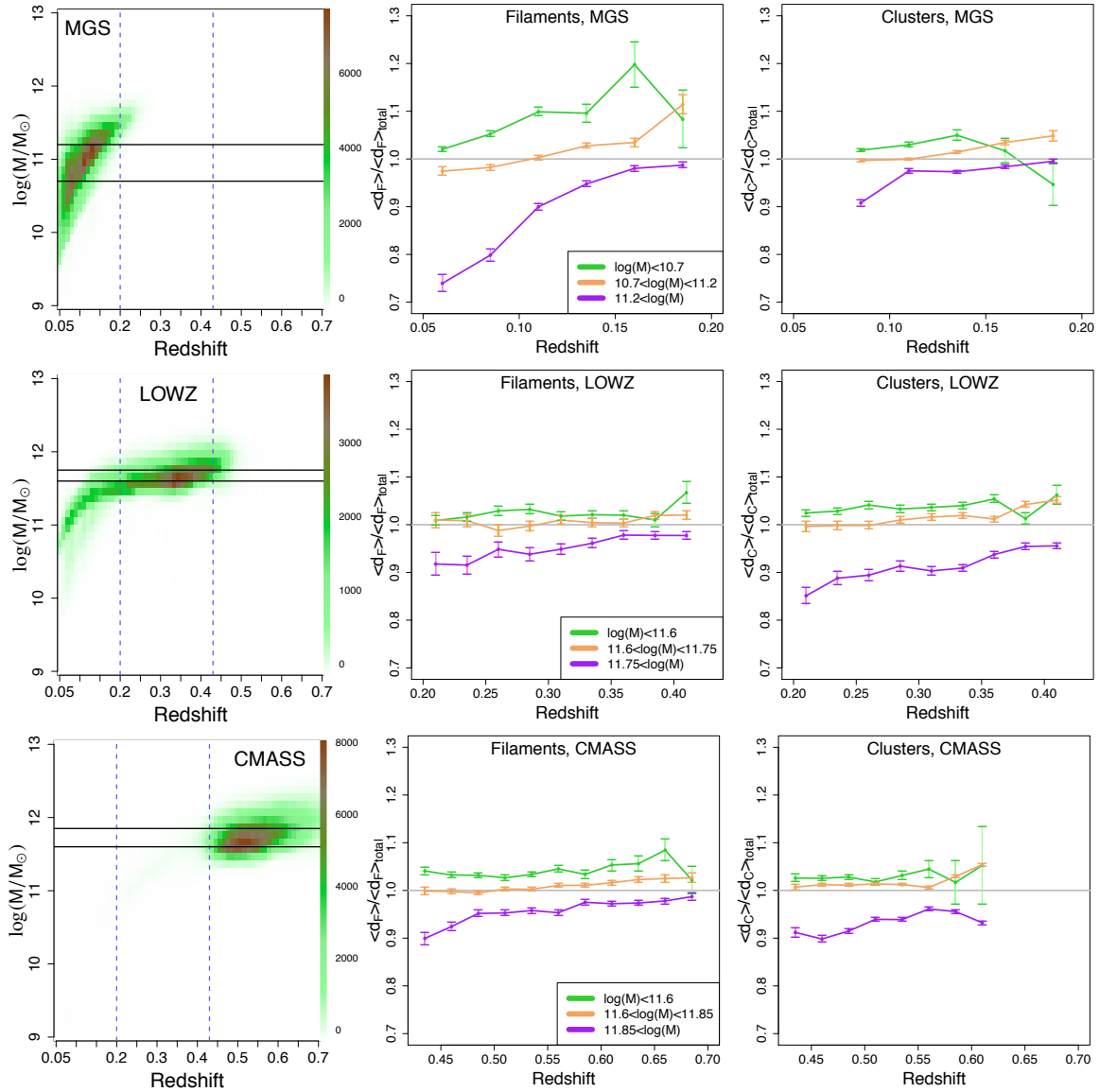


Figure 4. The correlation between a galaxy’s stellar mass and its proximity to filaments (and clusters). We separate galaxies according to their mass into three bins: low-mass galaxies (green color), moderate-mass galaxies (brown color), and high-mass galaxies (purple color). The top row of panels is the result for the MGS; the middle row is for LOWZ; the bottom row is for CMASS. **Left column:** the distribution of the logarithm of the stellar mass for galaxies. The two horizontal black lines indicate the boundaries for each mass bin. The two dashed vertical lines represent the boundaries for the three SDSS galaxy samples. **Center column:** Scaled distance from galaxies in different mass bins to filaments. **Right column:** Scaled distance from galaxies in different mass bins to clusters. There is a consistent trend in all panels of center and right columns: purple curves are lowest and green curves are highest. This means that heavy galaxies are closer to both filaments and clusters on average than light galaxies.

6 RESULTS: AGE

Besides color and stellar mass, the age of a galaxy is also found to be environment-dependent; see, e.g., (Bernardi et al. 1998; Trager et al. 2000; Wegner & Grogin 2008; Smith et al. 2012a). Generally, late-forming galaxies tend to reside in overdense regions (Sil’chenko 2006; Bernardi et al. 2006; Deng 2014). Based on this density-dependent relation to the age, we expect that late-forming galaxies will be closer to filaments than early-forming galaxies.

To assign an age to each SDSS galaxy, we use the best-fit mass-weighted average age of the stellar population of the

FSPS method (Conroy et al. 2009). The age distribution within each galaxy catalogue is given in the first column of Figure 5. There are many strips in the age distribution; this pattern arises because the FSPS method uses a grid of models, where age is a discrete variable.

Since a galaxy’s age and stellar mass are correlated, we partition galaxies according to their stellar mass within the same redshift slice to adjust the effect from stellar mass. For the MGS, we construct 30 even log-stellar mass bins ranging from 10.0 to 11.5 (in the unit of logarithm of solar mass and each bin has $\delta \log(M) = 0.05$); the LOWZ sample use 10 bins for the mass ranging from 11.5 to 12.0; the CMASS

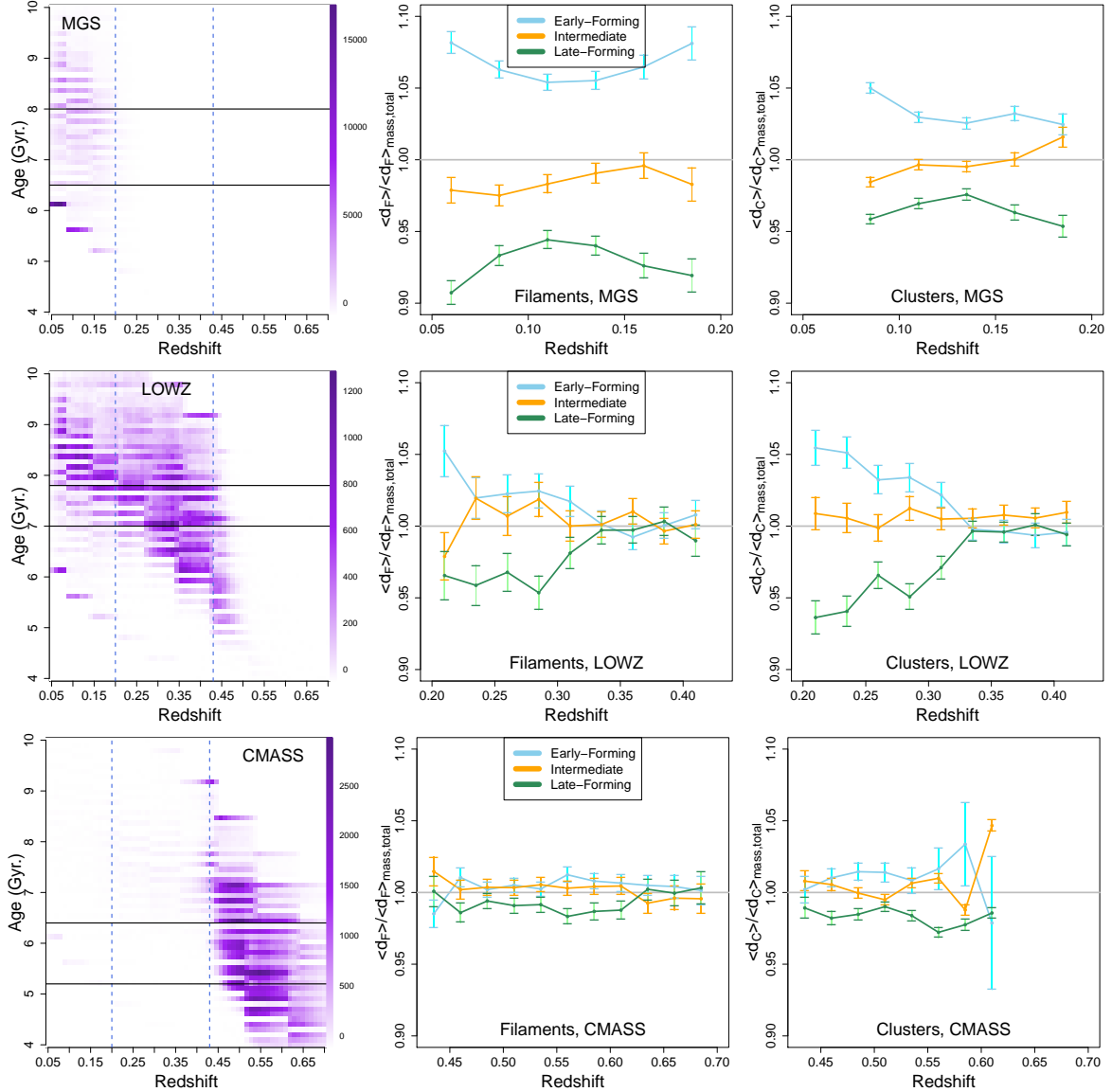


Figure 5. The correlation between a galaxy’s age and its proximity to filaments (and clusters). We partition galaxies into three age types: early-forming galaxies (light blue), intermediate-stage galaxies (orange), and late-forming galaxies (dark green). The top row of panles is the result for the MGS; the middle row is for LOWZ; the bottom row is for CMASS. **Left column:** the distribution of the age for galaxies. The top horizontal black lines indicate the boundaries for each age-type. The two horizontal black lines indicate the boundaries for each age-type. The two dashed vertical lines represents the boundaries for the three SDSS galaxy samples. **Center column:** Scaled distance from different age-type galaxies to filaments. **Right column:** Scaled distance from age-type galaxies to clusters. On the first row (MGS), there is a clear pattern that old galaxies (green curves) are closer to both the filaments and clusters than young galaxies (light blue curves) after adjusting the effect from stellar mass. In other catalogues, we still observe a similar pattern but the magnitude is much smaller than MGS, probably due to the low number density.

has 16 bins for the mass ranging from 11.5 to 12.3. Then we compute the average distance to filaments and clusters using all galaxies within the same mass bin and redshift slice. We denote these mass-adjusted average distance as $\langle d_F \rangle_{\text{mass, total}}$ and $\langle d_C \rangle_{\text{mass, total}}$; these quantities are used to normalize d_F and d_C for each galaxies within the specified mass and redshift range as equation (2).

After computing the scaled distance $d_F / \langle d_F \rangle_{\text{mass, total}}$ and $d_C / \langle d_C \rangle_{\text{mass, total}}$, we partition galaxies in each catalogue into three age-types: early-forming galaxies (light blue), intermediate-stage galaxies (orange), and late-forming

galaxies (dark green). Similar to the mass cuts, we choose the age cuts to balance the number of galaxies within each type. We conduct the same analysis as for color and stellar mass that compares scaled distance from each age-type of galaxy to filaments and clusters in each catalogue.

For the scaled distance to filaments (center column of Figure 5), every difference between results for galaxies with different formation times in the MGS is significant ($> 5\sigma$ by equation (4); see Table 2). We observe that late-forming galaxies tend to be closer to filaments compared to early-forming galaxies. For the LOWZ and the CMASS sam-

ple, there is no significant difference between early-forming and intermediate-stage galaxies but the intermediate-stage galaxies are significantly different to the late-forming galaxies ($> 3\sigma$) in terms of average distance to filaments. When we compare the center column to right column (cluster case), a similar pattern is observed but the cluster case has a more significant separation. Thus, the data suggest that there is correlation between a galaxy's age and its proximity to filaments (and clusters) after adjusting the effect from stellar mass. A possible scenario is that late-forming galaxies tend to sit at the centers of halos which will eventually become clusters or form filaments. We have not considered the color-age dependency and quenching; these are possible effects that could explain the age-proximity correlation.

7 RESULTS: SIZE

Finally, we investigate the relation of the size of a galaxy with its proximity to filaments. Similar to the color and the stellar mass, the size of a galaxy has also been found to be dependent on the environment (Cooper et al. 2012; Lani et al. 2013; Cappellari 2013; Kelkar et al. 2015). Hence, due to the properties of filaments, we expect to see a difference in the average distance to filaments from galaxies when we partition galaxies according to their size.

Our analysis focuses on the LOWZ sample since photometry in the CMASS sample is not as accurate as the LOWZ sample, and faint galaxies in MGS also suffer from this issue. The size adopted is the effective radius (R_e) obtained by fitting the de Vaucouleurs profile (de Vaucouleurs 1948). We partition galaxies into three groups by their size:

small galaxies (green) : $R_e < 5.6$ kpc

medium galaxies (brown) : $5.6 \text{ kpc} < R_e < 7.8$ kpc

large galaxies (purple) : $7.8 \text{ kpc} < R_e$.

We select two thresholds (4 and 6 kpc) to balance the number of galaxies within each size-type. The size distribution is presented in the left panel of Figure 6. Since stellar mass has influence over the average distance, we apply the mass-partitioning method in previous section to adjust the effect of stellar mass.

The results are presented in the center and right panels of Figure 6. There is a significant difference in average distance to filaments and clusters when large galaxies are compared to the other two types (significance $> 8\sigma$ by equation (4); see Table 2). This result indicates that, after adjusting the effect from stellar mass, large galaxies (purple) aggregate around filaments and clusters while small galaxies (green) tend to have a larger average distance from both filaments and clusters. We do not observe any significance for the difference between small and medium galaxies.

Our result is consistent with previous studies that galaxies that reside within denser environments tend to be larger (Lani et al. 2013; Cooper et al. 2012). A possible explanation for this effect is galaxy mergers. Mergers are more common in high-density environments so that if mergers are the dominating effect for the size growth of early-type massive galaxies, we should expect to see a correlation between density environment and the size of a galaxy (Cooper et al. 2012). Since filaments and clusters are tracers of high-density regions, a galaxy with a shorter distance to filaments

(or clusters) will have a higher density environment than galaxies located at a greater distance.

8 DISCUSSION

In this paper, we study the relationship of properties of a galaxy as a function of its distance to the nearest filaments (and clusters). We observe strong separations between different types of galaxies; table 2 summarizes the signal strengths for each catalogue (the MGS, LOWZ, and CMASS). For the MGS, the separations between types are significant among all comparisons. Differences with $> 5\sigma$ are present for all comparisons; some relations even have a $> 15\sigma$ significance. For the LOWZ sample, the results for stellar mass are significant ($> 3\sigma$). In the age and size cases, after adjusting the effect from stellar mass, we obtain significant correlations for intermediate-stage galaxies versus late-forming galaxies and medium galaxies versus large galaxies ($> 4\sigma$). In the CMASS sample, separating galaxies by stellar mass yields a highly significant result ($> 10\sigma$). When we consider the case of age, the result is similar to the LOWZ. Taking all evidence into account, our analysis provides evidence that several galaxy properties are correlated with filaments.

Our findings also include:

- (i) Several galaxy properties, including color, stellar mass, age, and size, are correlated with filaments. Our result is direct evidence for the correlation between filaments and the properties of galaxies (other results can be found in Guo et al. 2015; Alpaslan et al. 2015; Eardley et al. 2015). These correlation signals are expected since filaments trace the medium-to-high environmental density regions.
- (ii) Even in the high redshift regime ($z > 0.25$), we still detect a consistent correlation signal from many galaxy properties to filaments. Other analysis uses the Main galaxy sample, which focuses on the regions at $z \leq 0.25$ (Zhang et al. 2013; Tempel et al. 2014b; Guo et al. 2015). Filament analysis at high redshift ($z \geq 0.25$) has been done in some other surveys, see, e.g., Eardley et al. (2015); Alpaslan et al. (2015); our findings are consistent with theirs. These high redshift surveys, however, focus only on a small region of the sky.
- (iii) Filaments from Cosmic Web Reconstruction catalogue and reMaPPer galaxy clusters are similar in the sense that they have similar observed trends in galaxy properties near both filaments and clusters. This behavior shows the effectiveness of using density ridges as tracers of filaments. Prior to our work, no direct analysis of filament impacts on galaxy properties has been performed for the filaments from density ridges, although density ridges are similar to Voronoi filaments (Chen et al. 2015c) and have the desired statistical properties (Chen et al. 2014).

ACKNOWLEDGMENTS

We thank Hung-Jin Huang, Florent Leclercq, Peter Melchior, and Hy Trac for useful comments and discussions; we also thank Sukhdeep Singh for providing the de Vaucouleurs sizes for LOWZ sample. This work is supported in part by the Department of Energy under grant DESC0011114; YC is supported by William S. Dietrich II Presidential Ph.D. Fellowship; SH is supported in part by DOE-ASC, NASA

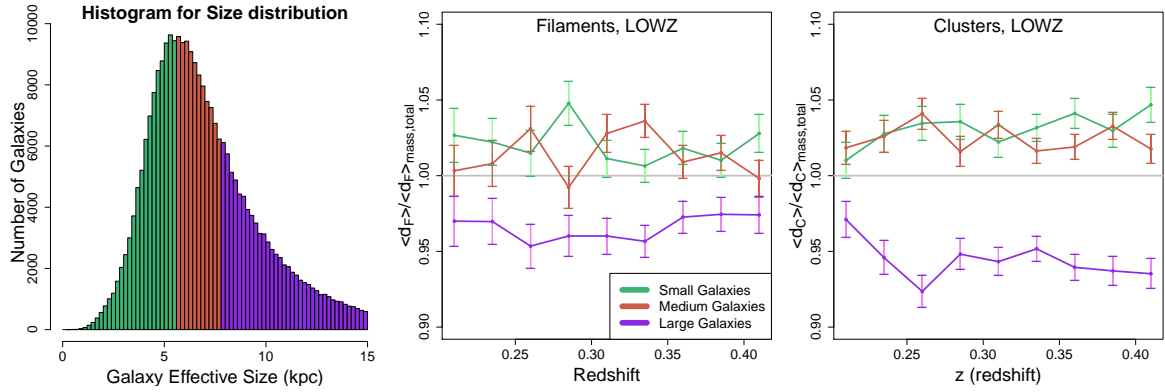


Figure 6. The correlation between a galaxy’s size and its proximity to filaments (and clusters). We partition galaxies into three types: small galaxies (green, $R_e < 5.6$ kpc), medium galaxies (dark orange, $5.6 \text{ kpc} < R_e < 7.8$ kpc), and large galaxies (purple, $7.8 \text{ kpc} < R_e$). **Left panel:** the age distribution for galaxies. The histogram is colored according to the three size. **Center panel:** Scaled distance from different size galaxies to filaments. **Right panel:** Scaled distance from different size galaxies to clusters. In both center and right panel, large galaxies (purple curves) are always lowest than other two size-types of galaxies after adjusting the effect from stellar mass, indicating that large galaxies tend to be closer to both filaments and clusters than small galaxies.

Separation	Type	MGS ($0.05 < z < 0.23$)	LOWZ ($0.23 < z < 0.43$)	CMASS ($0.43 < z < 0.70$)
Color	Red VS Blue	57.96σ	N/A	N/A
Stellar Mass	Low-mass VS Moderate-mass	15.65σ	3.72σ	11.04σ
	Moderate-mass VS High-mass	27.59σ	10.16σ	20.28σ
Age	Early-forming VS Intermediate-stage	5.59σ	0.15σ	0.95σ
	Intermediate-stage VS Late-forming	22.34σ	4.01σ	3.91σ
Size	Small VS Medium	N/A	1.20σ	N/A
	Medium VS Large	N/A	7.30σ	N/A

Table 2. Signal strength for the separation of galaxy distance to filaments according to the color, stellar mass, age, and size.

and NSF; RM is supported by the Alfred P. Sloan Foundation; CG is supported in part by DOE and NSF; LW is supported by NSF grant DMS1513412.

Funding for SDSS-III has been provided by the Alfred P. Sloan Foundation, the Participating Institutions, the National Science Foundation, and the U.S. Department of Energy Office of Science. The SDSS-III web site is <http://www.sdss3.org/>.

SDSS-III is managed by the Astrophysical Research Consortium for the Participating Institutions of the SDSS-III Collaboration including the University of Arizona, the Brazilian Participation Group, Brookhaven National Laboratory, Carnegie Mellon University, University of Florida, the French Participation Group, the German Participation Group, Harvard University, the Instituto de Astrofísica de Canarias, the Michigan State/Notre Dame/JINA Participation Group, Johns Hopkins University, Lawrence Berkeley National Laboratory, Max Planck Institute for Astrophysics, Max Planck Institute for Extraterrestrial Physics, New Mexico State University, New York University, Ohio State University, Pennsylvania State University, University of Portsmouth, Princeton University, the Spanish Participation Group, University of Tokyo, University of Utah, Vanderbilt University, University of Virginia, University of Washington, and Yale University.

REFERENCES

- Abazajian K. N., et al., 2009, *ApJS*, **182**, 543
Adelman-McCarthy J. K., et al., 2008, *ApJS*, **175**, 297
Aihara H., et al., 2011, *ApJS*, **193**, 29
Alam S., et al., 2015, *ApJS*, **219**, 12
Alpaslan M., et al., 2015, preprint, ([arXiv:1505.05518](https://arxiv.org/abs/1505.05518))
Altay G., Colberg J. M., Croft R. A. C., 2006, *MNRAS*, **370**, 1422
Anderson L., et al., 2012, *MNRAS*, **427**, 3435
Anderson L., et al., 2014a, *MNRAS*, **439**, 83
Anderson L., et al., 2014b, *MNRAS*, **441**, 24
Aragon-Calvo M. A., Yang L. F., 2014, *MNRAS*, **440**, L46
Aragon-Calvo M. A., Jones B. J. T., van de Weygaert R., van der Hulst J. M., 2007, *A&A*, **474**, 315
Aragon-Calvo M. A., van de Weygaert R., Jones B. J. T., 2010, *MNRAS*, **408**, 2163
Balogh M. L., Baldry I. K., Nichol R., Miller C., Bower R., Glazebrook K., 2004, *ApJ*, **615**, L101
Bernardi M., Renzini A., da Costa L. N., Wegner G., Alonso M. V., Pellegrini P. S., Rité C., Willmer C. N. A., 1998, *ApJ*, **508**, L143
Bernardi M., Nichol R. C., Sheth R. K., Miller C. J., Brinkmann J., 2006, *AJ*, **131**, 1288
Blanton M. R., Lin H., Lupton R. H., Maley F. M., Young N., Zehavi I., Loveday J., 2003, *AJ*, **125**, 2276
Blanton M. R., et al., 2005a, *AJ*, **129**, 2562

- Blanton M. R., Eisenstein D., Hogg D. W., Schlegel D. J., Brinkmann J., 2005b, *ApJ*, **629**, 143
- Bolton A. S., et al., 2012, *AJ*, **144**, 144
- Bond J. R., Kofman L., Pogosyan D., 1996, *Nature*, **380**, 603
- Bond N. A., Strauss M. A., Cen R., 2010, *MNRAS*, **409**, 156
- Bower R. G., Lucey J. R., Ellis R. S., 1992, *MNRAS*, **254**, 601
- Butcher H., Oemler Jr. A., 1978, *ApJ*, **226**, 559
- Cappellari M., 2013, *ApJ*, **778**, L2
- Cautun M., van de Weygaert R., Jones B. J. T., 2013, *MNRAS*, **429**, 1286
- Chen Y.-C., Genovese C. R., Wasserman L., 2014, preprint, ([arXiv:1406.5663](https://arxiv.org/abs/1406.5663))
- Chen Y.-C., Ho S., Freeman P. E., Genovese C. R., Wasserman L., 2015a, Cosmic Web Reconstruction through Density Ridges: Catalogue, In preparation
- Chen Y.-C., Ho S., Freeman P. E., Genovese C. R., Wasserman L., 2015c, preprint, ([arXiv:1501.05303](https://arxiv.org/abs/1501.05303))
- Chen Y.-C., et al., 2015b, preprint, ([arXiv:1508.04149](https://arxiv.org/abs/1508.04149))
- Christlein D., Zabludoff A. I., 2005, *ApJ*, **621**, 201
- Codis S., et al., 2015, *MNRAS*, **448**, 3391
- Coil A. L., et al., 2008, *ApJ*, **672**, 153
- Conroy C., Gunn J. E., White M., 2009, *ApJ*, **699**, 486
- Cooper M. C., et al., 2012, *MNRAS*, **419**, 3018
- Cowan N. B., Ivezić Ž., 2008, *ApJ*, **674**, L13
- Darvish B., Sobral D., Mobasher B., Scoville N. Z., Best P., Sales L. V., Smail I., 2014, *ApJ*, **796**, 51
- Dawson K. S., et al., 2013, *AJ*, **145**, 10
- Deng X.-F., 2014, Bulletin of the Astronomical Society of India, **42**, 59
- Desjacques V., 2008, *MNRAS*, **388**, 638
- Doi M., et al., 2010, *AJ*, **139**, 1628
- Dubois Y., et al., 2014, *MNRAS*, **444**, 1453
- Eardley E., et al., 2015, *MNRAS*, **448**, 3665
- Eberly D., 1996, Ridges in Image and Data Analysis. Springer
- Eisenstein D. J., et al., 2011, *AJ*, **142**, 72
- Font A. S., et al., 2008, *MNRAS*, **389**, 1619
- Fukugita M., Ichikawa T., Gunn J. E., Doi M., Shimasaku K., Schneider D. P., 1996, *AJ*, **111**, 1748
- Genovese C. R., Perone-Pacífico M., Verdinelli I., Wasserman L., 2014, The Annals of Statistics, **42**, 1511
- González R. E., Padilla N. D., 2009, *MNRAS*, **397**, 1498
- Grützbauch R., Conselice C. J., Varela J., Bundy K., Cooper M. C., Skibba R., Willmer C. N. A., 2011, *MNRAS*, **411**, 929
- Gunn J. E., et al., 1998, *AJ*, **116**, 3040
- Gunn J. E., et al., 2006, *AJ*, **131**, 2332
- Guo Q., et al., 2011, *MNRAS*, **413**, 101
- Guo Q., Tempel E., Libeskind N. I., 2015, *ApJ*, **800**, 112
- Hahn O., Porciani C., Carollo C. M., Dekel A., 2007a, *MNRAS*, **375**, 489
- Hahn O., Carollo C. M., Porciani C., Dekel A., 2007b, *MNRAS*, **381**, 41
- Hogg D. W., et al., 2003, *ApJ*, **585**, L5
- Jasche J., Kitaura F. S., Li C., Enßlin T. A., 2010, *MNRAS*, **409**, 355
- Joachimi B., Singh S., Mandelbaum R., 2015, preprint, ([arXiv:1504.02662](https://arxiv.org/abs/1504.02662))
- Kauffmann G., White S. D. M., Heckman T. M., Ménard B., Brinchmann J., Charlot S., Tremonti C., Brinkmann J., 2004, *MNRAS*, **353**, 713
- Kelkar K., Aragón-Salamanca A., Gray M. E., Maltby D., Vulcani B., De Lucia G., Poggianti B. M., Zaritsky D., 2015, *MNRAS*, **450**, 1246
- Lagos C. D. P., Padilla N. D., Cora S. A., 2009, *MNRAS*, **395**, 625
- Lani C., et al., 2013, *MNRAS*, **435**, 207
- Leclercq F., Jasche J., Wandelt B., 2015, *J. Cosmology Astropart. Phys.*, **6**, 15
- Lupton R., Gunn J. E., Ivezić Z., Knapp G. R., Kent S., 2001, in Harnden Jr. F. R., Primini F. A., Payne H. E., eds, Astronomical Society of the Pacific Conference Series Vol. 238, Astronomical Data Analysis Software and Systems X. p. 269 ([arXiv:astro-ph/0101420](https://arxiv.org/abs/astro-ph/0101420))
- Maraston C., et al., 2013, *MNRAS*, **435**, 2764
- Moster B. P., Somerville R. S., Maubetsch C., van den Bosch F. C., Macciò A. V., Naab T., Oser L., 2010, *ApJ*, **710**, 903
- Novikov D., Colombi S., Doré O., 2006, *MNRAS*, **366**, 1201
- Ozertem U., Erdogmus D., 2011, *JMLR*, **12**, 1249
- Padmanabhan N., et al., 2008, *ApJ*, **674**, 1217
- Park C., Choi Y.-Y., Vogeley M. S., Gott III J. R., Blanton M. R., SDSS Collaboration 2007, *ApJ*, **658**, 898
- Pier J. R., Munn J. A., Hindsley R. B., Hennessy G. S., Kent S. M., Lupton R. H., Ivezić Ž., 2003, *AJ*, **125**, 1559
- Robertson B., Bullock J. S., Font A. S., Johnston K. V., Hernquist L., 2005, *ApJ*, **632**, 872
- Rozo E., Rykoff E. S., 2014, *ApJ*, **783**, 80
- Rozo E., Rykoff E. S., Bartlett J. G., Melin J.-B., 2015, *MNRAS*, **450**, 592
- Rykoff E. S., et al., 2014, *ApJ*, **785**, 104
- Sil'chenko O. K., 2006, *ApJ*, **641**, 229
- Smee S. A., et al., 2013, *AJ*, **146**, 32
- Smith R. J., Lucey J. R., Price J., Hudson M. J., Philipps S., 2012a, *MNRAS*, **419**, 3167
- Smith A. G., Hopkins A. M., Hunstead R. W., Pimbblet K. A., 2012b, *MNRAS*, **422**, 25
- Sousbie T., 2011, *MNRAS*, **414**, 350
- Sousbie T., Pichon C., Colombi S., Novikov D., Pogosyan D., 2008a, *MNRAS*, **383**, 1655
- Sousbie T., Pichon C., Courtois H., Colombi S., Novikov D., 2008b, *ApJ*, **672**, L1
- Springel V., et al., 2005, *Nature*, **435**, 629
- Stoica R. S., Martínez V. J., Mateu J., Saar E., 2005, *A&A*, **434**, 423
- Stoica R. S., Martínez V. J., Saar E., 2007, *JRSSC*, **56**, 459
- Strauss M. A., et al., 2002, *AJ*, **124**, 1810
- Tempel E., Libeskind N. I., 2013, *ApJ*, **775**, L42
- Tempel E., Stoica R. S., Saar E., 2013, *MNRAS*, **428**, 1827
- Tempel E., Libeskind N. I., Hoffman Y., Liivamägi L. J., Tamm A., 2014a, *MNRAS*, **437**, L11
- Tempel E., Stoica R. S., Martínez V. J., Liivamägi L. J., Castellan G., Saar E., 2014b, *MNRAS*, **438**, 3465
- Tempel E., Guo Q., Kipper R., Libeskind N. I., 2015, *MNRAS*, **450**, 2727
- Trager S. C., Faber S. M., Worthey G., González J. J., 2000, *AJ*, **120**, 165
- Wegner G., Grogin N. A., 2008, *AJ*, **136**, 1
- York D. G., et al., 2000, *AJ*, **120**, 1579
- Zhang Y., Yang X., Wang H., Wang L., Mo H. J., van den Bosch F. C., 2013, *ApJ*, **779**, 160

Zhang Y., Yang X., Wang H., Wang L., Luo W., Mo H. J.,
van den Bosch F. C., 2015, [ApJ](#), **798**, 17
de Vaucouleurs G., 1948, Annales d'Astrophysique, **11**, 247

This paper has been typeset from a \LaTeX file prepared
by the author.